RSC Advances

ROYAL SOCIETY OF CHEMISTRY

PAPER

View Article Online
View Journal | View Issue

Check for updates

Cite this: *RSC Adv.*, 2024, **14**, 12593

Significantly enhanced catalytic performance of Pd nanocatalyst on AlOOH featuring abundant solid surface frustrated Lewis pair for improved hydrogen activation†

Junwei Li,[a] Hongshuai Yin,[a] Sisi Liu,[a] Chaofa Xu *[ab] and Zhixiong Cai [ab]

Received 10th March 2024
Accepted 11th April 2024

DOI: 10.1039/d4ra01852d

rsc.li/rsc-advances

The catalytic performance of a catalyst is significantly influenced by its ability to activate hydrogen. Constructing frustrated Lewis pairs (FLPs) with the capacity for hydrogen dissociation on non-reducible supports remains a formidable challenge. Herein, we employed a straightforward method to synthesize a layered AlOOH featuring abundant OH defects suitable for constructing solid surface frustrated Lewis pair (ssFLP). The results indicated that the AlOOH-80 (synthesized at 80 °C) possessed an appropriate crystalline structure conducive to generating numerous OH defects, which facilitated the formation of ssFLP. This was further evidenced by the minimal water adsorption in the AlOOH-80, inversely correlated with the quantity of defects in the catalyst. As expected, the Pd loaded onto AlOOH (Pd/AlOOH-80) exhibited excellent catalytic activity in hydrogenation reactions, attributed to abundant defects available for constructing ssFLP. Remarkably, the Pd/AlOOH-80 catalyst, with larger-sized Pd nanoparticles, displayed notably superior activity compared to commercial Pd/Al_2O_3 and Pd/C, both featuring smaller-sized Pd nanoparticles. Evidently, under the influence of ssFLP, the size effect of Pd nanoparticles did not dominate, highlighting the pivotal role of ssFLP in enhancing catalytic performance. This catalyst also exhibited exceptionally high stability, indicating its potential for industrial applications.

1. Introduction

Catalytic hydrogenation reactions hold significant importance in the petrochemical industry. Given that most of these processes rely on catalysts, therefore, the rational design of hydrogenation catalysts has garnered growing attention.[1–3] The activation method of hydrogen is crucial, making it impossible to ignore when designing catalysts. During the catalytic process, hydrogen undergoes dissociation by noble metals, transition metals, and even carbon.[4–6] However, a novel and unconventional approach to hydrogen dissociation is attracting growing attention, incorporating the utilization of frustrated Lewis pair (FLP).[7,8] This represents a distinctive method of hydrogen dissociation and relies significantly on the proximity distance between the Lewis acid and base sites.[9,10]

Controlling the distance between the Lewis acid and base sites is easy in homogeneous catalysts, which is why most FLP hydrogen dissociation behaviors occur in homogeneous catalytic systems. D. W. Stephan first reported the dissociation of H_2 by controlling this distance, demonstrating that FLP could activate H_2.[11] Early research on FLP was primarily based on these homogeneous catalysts. Undoubtedly, the inability to recover homogeneous catalysts is the greatest obstacle to the application of this type of catalys.[12–15] Fortunately, for heterogeneous catalysts, it is also possible to achieve the formation of FLP under specific conditions. This also suggests that the dissociation of hydrogen by FLP is achievable under specific conditions. Moreover, most FLPs are constructed on reducible supports because they can easily form defects, such as oxygen vacancies. This indicates that surface defects on supports are crucial for the formation of FLP.[16–18] For example, Ozin constructed FLP on the surface of $In_2O_{3-x}(OH)_y$ through surface hydroxyl groups (Lewis bases) and indium (Lewis acids), demonstrating that the FLPs facilitated the adsorption and dissociative splitting of H_2 in the photocatalytic Reverse Water Gas Shift reaction (RWGS).[19] However, for non-reducible metal oxides, there remained significant challenges. Constructing FLPs on non-reducible metal oxides remains a significant challenge due to the difficulty in generating defects through redox processes. In 2022, H. Z. Liu and colleagues were the first to successfully construct solid surface frustrated Lewis pair (ssFLP) on the non-reducible hydroxide (AlOOH). They found

[a]College of Chemistry, Chemical Engineering and Environment, Minnan NormalUniversity, Zhangzhou 363000, China. E-mail: xuchaofa@mnnu.edu.cn
[b]Fujian Province Key Laboratory of Modern Analytical Science and Separation Technology, Minnan Normal University, Zhangzhou 363000, China

† Electronic supplementary information (ESI) available. See DOI: https://doi.org/10.1039/d4ra01852d

that the Lewis basic O_{Hv} site (one H removed from OH) and an adjacent Lewis acidic unsaturated Al site ($Al_{unsat.}^{3+}$) proximal to a surface OH_v on AlOOH layers could form the ssFLP.[20] Interestingly, even without metals capable of dissociating hydrogen, ssFLP could still dissociate hydrogen and be applied in the hydrogenation of alkynes under mild conditions. This provided new insights for the design of hydrogenation catalysts, beneficial for the development of novel and efficient hydrogenation catalysts.

In this work, we employed a straightforward methodology to directly synthesize layered AlOOH enriched with ssFLPs on its surface. After loading Pd onto AlOOH, the resulting Pd/AlOOH catalyst exhibited remarkable catalytic performance, surpassing even commercial Pd/Al_2O_3 and Pd/C. Furthermore, the catalytic efficiency of Pd-based catalysts exhibited a direct relationship with the number of OH defects on the AlOOH surface while inversely relating to the quantity of adsorbed water. Pd/AlOOH-80 exhibited excellent catalytic performance, thanks to its low surface water content, implying more OH defect sites on the surface, thereby enabling the easier formation of ssFLPs. Building upon the capacity of ssFLPs to dissociate hydrogen, the hydrogen dissociation ability of Pd/AlOOH-80 had been enhanced, leading to a synergistic effect between Pd and AlOOH-80, thereby improving the catalytic performance of the catalyst. In addition to its excellent catalytic performance, Pd/AlOOH-80 also exhibited good reusability, with no significant decline in catalytic performance observed over five cycles of experiments, indicating its high potential for industrial applications.

2. Materials and methods

2.1. Chemical materials

Commercial Pd/C (5 wt%), commercial Pd/Al_2O_3 and palladium chloride was purchased from energy chemical. Hydrochloric acid (36–38%), ethanol, pyridine, benzoic acid, silicon dioxide, aluminium oxide and titanium dioxide were purchased from Xilong Scientific Co., Ltd. Phenylacetylene (PLE, 97%) was purchased from Aladdin. H_2 (99.999%) was purchased from Haolilai Gas Co. Ltd. The water used in all experiment was deionized water (18.2 MΩ). All chemicals were used as received without further purification.

2.2. Catalyst preparation

2.2.1 Preparation of AlOOH with different synthesis conditions. In a typical synthesis of AlOOH-80, 25 mmol of sodium aluminate and 25 mmol of ammonium chloride were dissolved in 100 mL and 25 mL of deionized water, respectively. The ammonium chloride solution was then added to the sodium aluminate solution. The mixture was stirred at 80 °C for 10 minutes. The white products were collected by centrifugation and washed with ethanol for several times. Finally, the products were dried in a vacuum oven at 60 °C for 12 h (AlOOH-80). The steps of adding sodium aluminate, ammonium chloride, and acetic acid were repeated, but the mixture was stirred at room temperature for 10 minutes, referred to as AlOOH-RT. AlOOH-RT was transferred to a 100 mL polytetrafluoroethylene-lined stainless-steel autoclave, and then subjected to solvothermal treatment at 180 °C for 5 hours, referred to as AlOOH-SS (schematic of the synthesis as shown in Fig. S1†).

2.2.2 Preparation of Pd/AlOOH. $PdCl_2$ was reacted with HCl at 70 °C for 1 hour to produce a 1 mol L^{-1} H_2PdCl_4 aqueous solution, which was then diluted to 0.01 mol L^{-1}. In a glass pressure vessel, 100 mg of AlOOH was added followed by the addition of 50 mL of deionized water, and the mixture was homogenized using ultrasound. At 50 °C and 420 rpm, 652 μL of the H_2PdCl_4 solution (0.01 M) was added dropwise (the loading of Pd was 0.7 wt%), while continuously introducing H_2 gas at 0.1 MPa. After 1 hour, the catalyst was collected using a centrifuge and washed three times with deionized water. The synthesis steps for the palladium-loaded catalysts mentioned later, except for the different supports used, were entirely consistent with this procedure.

2.3. Catalytic evaluations

Pd/AlOOH-RT, Pd/AlOOH-80, Pd/AlOOH-SS, Pd loaded on other supports, and commercial catalysts were first dispersed in ethanol. Then, the alkyne was taken for the catalytic reaction based on the required amount of catalyst. Typically, for a 1 : 3000 (Pd/PhC≡CH) ratio, 1.6 μmol of Pd was used for the hydrogenation reaction of phenylacetylene. In a glass pressure vessel, the catalyst was dispersed in 10 mL of ethanol, ultrasonicated for 5 minutes, and then mixed with 4.8 mmol of PhC≡CH under magnetic stirring. After purging the reaction vessel with H_2, H_2 was continuously fed into the container, and the mixture was stirred in a 30 °C water bath. The reaction was allowed to proceed for a certain time before a small portion of the solution was withdrawn for analysis by GC.

2.4. Characterizations

Thermogravimetric analysis (TGA) of the samples was performed using a NETZSCH STA 449F5 thermogravimetric analyzer, with a heating program from 25 °C to 1000 °C under air atmosphere at a heating rate of 10 °C min^{-1}. The powder X-ray diffraction (XRD) patterns of the samples were performed on Rigaku Ultima IV diffractometer using Cu Kα X-ray source (40 kV). The surface elements and valence states were detected by X-ray photoelectron spectroscopy (XPS, Thermo ESCALAB 250XI). According to the N_2 adsorption–desorption isotherms, the specific surface area and particle size were obtained by Brunauer–Emmett–Teller (BET, Micromeritics Gemini 2390) method. Fourier-transformed infrared (FT-IR) spectra of samples was measured by a Thermo Nicolet spectrometer. The yields of corresponding products were determined by GC (Shimadzu GC-2010Plus) furnished with a flame ionization detector. ^{27}Al solid-state NMR (ssNMR) spectra were recorded on a JNM-ECZ600R 600 spectrometer equipped with a 3.2 mm tube diameter. The corresponding resonance frequency and magic angle spinning rate were 156 MHz and 12 kHz respectively. ^{27}Al ssNMR measurements were performed without any pretreatment on the samples. Pyridine adsorption experiment: AlOOH (50 mg) was mixed in ethanol (10 mL) with pyridine (1 mL), stirred at 30 °C for 2 hours, then centrifuged and ethanol-washed to remove physically adsorbed pyridine. The obtained sample was dried in an oven at 60 °C for 12 hours before being used for FTIR characterization.

3. Results and discussion

3.1. Surface structure characterizations of catalyst

As is known, the defects on the catalyst surface are directly related to its crystalline state.[21–25] The low crystallinity of AlOOH results in incomplete formation of a layered structure, limiting the creation of OH defects. Conversely, high crystallinity leads to a more perfect crystal structure with fewer surface defects. Therefore, maintaining AlOOH crystallinity at an optimal level ensures the presence of a maximum number of OH defects, crucial for forming ssFLPs. We characterized the catalyst using powder X-ray diffraction (XRD), and the results were shown in Fig. 1. Although the crystallinity of the three samples was different, the obtained diffraction peaks matched the diffraction peaks of AlOOH (JCPDS 21-1307) (Fig. 1a).[26] The diffraction peaks at $2\theta = 14.5°$, 28.2° and 38.3° were respectively attributed to the (020), (120), and (031) crystal planes of AlOOH (Fig. 1a). The XRD diffraction peak intensity of AlOOH-RT was the weakest, indicating its low crystallinity. This hindered the formation of a layered structure, resulting in fewer OH defects and making it difficult to form frustrated Lewis pairs on the solid surface.[27] In contrast, AlOOH-SS had the strongest XRD diffraction peak intensity, suggesting good crystallinity and fewer defects, which also hindered the formation of ssFLP. Excitingly, the XRD diffraction peaks of AlOOH-80 were within an appropriate range, indicating that its crystallinity maintained a balance, ensuring the presence of a layered structure while also maintaining a certain amount of defects.

In the pyridine adsorption experiment with AlOOH-80, we observed a significant infrared absorption peak at 1647 cm^{-1}, indicating interaction between the unsaturated Al sites (Lewis acid sites) and pyridine (Fig. S2†), potentially confirming the existence of ssFLP in AlOOH-80.[28] This observation highlights the favorable conditions for ssFLP production in AlOOH-80 facilitated by the presence of OH defects. Given its abundant OH defects available for constructing ssFLPs, one could reasonably anticipate AlOOH-80 to deliver superior catalytic performance. Following Pd loading, the diffraction peaks in the catalysts (Fig. 1b) remained virtually indistinguishable from those before loading, exhibiting no observable substantial modifications. Further, no diffraction peaks associated with Pd were detected, largely attributed to the minimal Pd loading (0.7 wt%).[29,30]

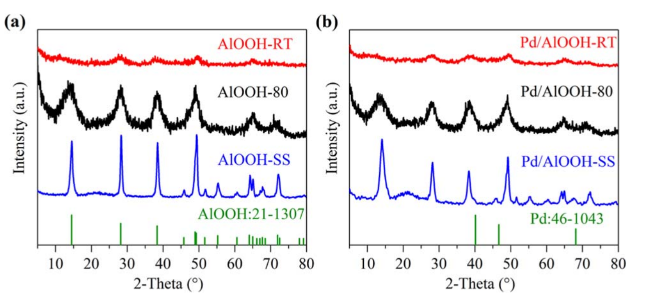

Fig. 1 XRD patterns of catalysts before (a) and after (b) Pd loading onto varying AlOOH matrix.

The morphology of the catalyst was explored using transmission electron microscopy (TEM). As illustrated in the TEM images (Fig. 2a), AlOOH-80 possessed a flower-like structure, built from lamellar units. HR-TEM images (Fig. 2b) showed the lattice fringes of AlOOH-80 at high magnification, where the lattice spacing of the magnified area was 0.235 nm, corresponding to the (031) crystal plane of AlOOH.[31] Combined with the results from XRD, it becomes clear that AlOOH-80 was an AlOOH with a layered structure bearing abundant OH defects, which was beneficial for the formation of ssFLP.[32] The specific surface area and pore size distribution of the catalyst were obtained through physical adsorption measurements. The N_2 isotherm adsorption–desorption curve of the AlOOH-80 catalyst exhibited type IV with a hysteresis loop at high relative pressures, indicating that the AlOOH possessed a mesoporous structure with a specific surface area of 428.7 $m^2\ g^{-1}$, with the pore size mainly distributed around 2.8 nm (Fig. S3†).[33–35] After Pd loading, the layered structure of the Pd/AlOOH-80 was preserved, suggesting no destruction occurred on the original layered structure (Fig. 2c). This circumstance facilitated the Pd/AlOOH-80 catalyst in developing ssFLP through the existence of OH defects. Simultaneously, we also observed that the Pd nanoparticles in the Pd/AlOOH-80 catalyst are uniformly

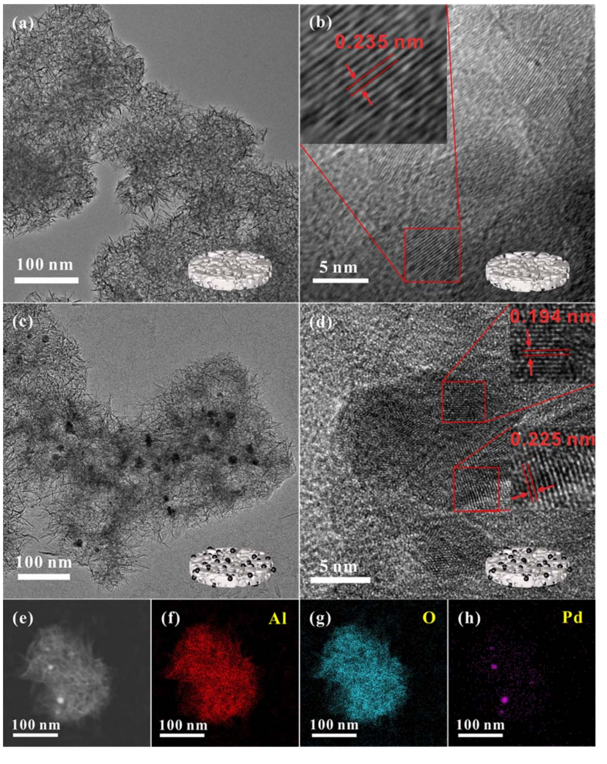

Fig. 2 (a) TEM image and (b) HR-TEM image of AlOOH-80; (c) TEM image and (d) HR-TEM image of Pd/AlOOH-80 and EDX mapping images of Pd/AlOOH-80 (e–h).

distributed over AlOOH, with a nanoparticle size of approximately 20 nm. HR-TEM images (Fig. 2d) displayed lattice spacings of 0.194 nm and 0.225 nm, respectively attributed to the (200) and (111) crystal planes of Pd.[27,28] Furthermore, the EDS mapping showed that Pd nanoparticles were uniformly dispersed on AlOOH-80 (Fig. 2e–h). This indicates that Pd nanoparticles were successfully loaded onto AlOOH-80, despite the lack of Pd information in the XRD diffraction peaks.

XPS was utilized to analyze the composition and valence states of elements on the surface of the catalyst, as shown in Fig. 3a. AlOOH-RT, AlOOH-80, and AlOOH-SS exhibited single peaks in their high-resolution Al 2p XPS spectra at binding energies of 74.2 eV, 74.1 eV, and 74.2 eV, respectively. Notably, compared to AlOOH-RT and AlOOH-SS, the Al 2p binding energy of AlOOH-80 was lower, which was due to the electron-rich $Al_{unsatur.}^{3+}$ caused by surface OH defects.[36,37] The fitted O 1s spectra of AlOOH-RT, AlOOH-80, and AlOOH-SS exhibited three peaks at 529.4–529.8, 530.8–531.2 and 532.1–532.9 eV, respectively(Fig. 3b). These peaks were attributed to oxygen in the lattice structure Al–O–Al (O_L), hydroxyl groups bound to Al forming Al–OH ($-OH_{Al-OH}$) or surface OH defects adsorbing oxygen (O_{ad}, $-OH_{ad}$), and adsorbed water (O_{adH2O}).[38] The results showed that the O_{adH_2O}/O_{Total} ratios for AlOOH-80, AlOOH-RT, and AlOOH-SS were 8.7%, 17.2% and 22.5%, respectively (Table S1†). Clearly, the quantity of adsorbed water (O_{adH_2O}) on AlOOH-80 is less than that on both AlOOH-RT and AlOOH-SS. The integration of the peak areas at this position, which was closely related to catalytic performance, will be discussed in detail later.

At the same time, the high-resolution Pd 3d XPS spectra of Pd/AlOOH-80 showed two peaks at 340.7 eV and 335.3 eV (Fig. 3c), corresponding to Pd $3d_{5/2}$ and Pd $3d_{3/2}$, respectively, indicating that Pd in Pd/AlOOH-80 was predominantly metallic palladium.[39–41] The FTIR spectra of AlOOH, displayed in Fig. 3d, showed a strong and broad absorption band at 3400 cm^{-1} for all samples, attributed to the stretching vibrations of free OH, possibly originating from hydroxyl groups connected by hydrogen bonds or adsorbed wate.[42] The absorption peak at 1610 cm^{-1} could be attributed to the bending vibration of surface OH or adsorbed water.[38] The peaks at 3088 cm^{-1} and 1071 cm^{-1} were attributed to the tensile and bending vibration modes of $-OH_{Al-OH}$, which further confirmed the existence of AlOOH.[43]

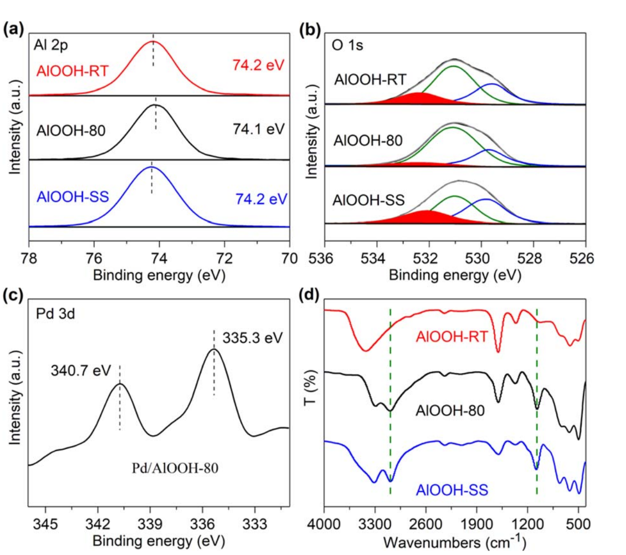

Fig. 3 (a) Al 2p and (b) O 1s XPS spectra of AlOOH; (c) Pd 3d XPS spectrum of Pd/AlOOH-80; (d) FTIR spectra of AlOOH.

The thermal gravimetric analysis (TGA) curve of AlOOH (Fig. 4a) exhibited two weight loss stages. The first stage began at room temperature and tended toward stabilization by 100 °C, corresponding to the loss of physically adsorbed water. Our observations revealed that AlOOH-80 incurred a 3.9% mass loss at this stage, which was much less than AlOOH-RT (12.4%) and AlOOH-SS (10.2%). This result was in great agreement with the XPS data, both demonstrating that AlOOH-80 had the least amount of water absorption on its surface. The second stage, starting after the adsorbed water was completely lost, approached stabilization around 480 °C and was attributed to the weight loss of hydroxyl groups bonded to the Al ($-OH_{Al-OH}$), namely, the dehydroxylation of AlOOH.[42] We employed ssNMR to characterize the coordination environment of AlOOH. As revealed by the ssNMR spectra, no peaks were displayed near 66 ppm or 36 ppm in AlOOH, indicating that Al exists in a six-coordination form in all AlOOH samples. The chemical shifts for AlOOH-80, AlOOH-RT, and AlOOH-SS were 10.1 ppm, 10.2 ppm, and 10.5 ppm, respectively. AlOOH-80 showed a higher chemical shift field, which was attributed to the electronic shielding effect of the abundant OH defects on the Al nucleus.[37,44]

3.2. Catalytic performances of catalysts

The catalytic performance of the catalysts was evaluated using the hydrogenation reaction of phenylacetylene as a model reaction. As shown in Fig. 5a, Pd/AlOOH-80 could completely hydrogenate phenylacetylene within 40 minutes, whereas Pd/AlOOH-RT and Pd/AlOOH-SS required 60 minutes and 100 minutes, respectively. Unmistakably, the catalytic activity of Pd/AlOOH-80 was significantly higher than that of Pd/AlOOH-RT and Pd/AlOOH-SS, consistent with the material characterization results.[45] As expected, Pd/AlOOH-80, resulting from Pd loaded onto AlOOH-80, was significantly higher than that of other catalysts on various oxide supports (Fig. 5b), even exceeding commercial Pd/C (Fig. S4†). After quantifying the Pd

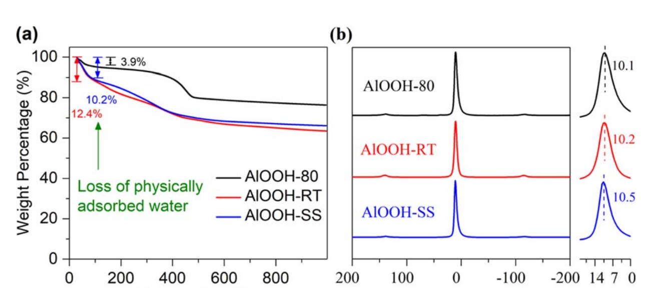

Fig. 4 (a) TGA analysis and (b) ^{27}Al ssNMR of AlOOH.

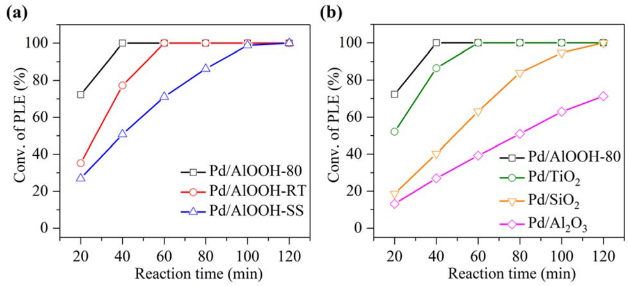

Fig. 5 Catalytic performance of (a) Pd loaded on AlOOH synthesized *via* different methods and (b) Pd loaded on various supports.

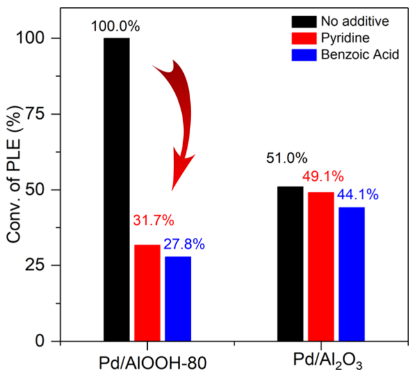

Fig. 6 Catalytic performance of catalysts before and after adding pyridine or benzoic. Reaction conditions: $P(H_2) = 0.1$ MPa, $T = 30$ °C, reaction time = 40 min, Pd = 1.6 μmol, phenylacetylene = 4.8 mmol, ethanol = 10 mL, 1.25 mmol of pyridine/benzoic acid was added to the reaction system.

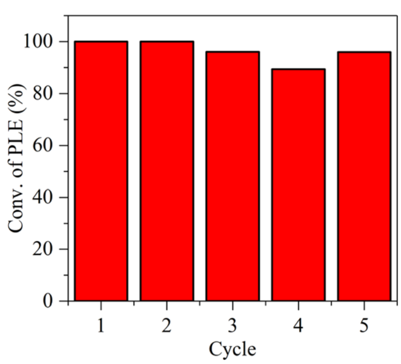

Fig. 7 Catalyst recycling of Pd/AlOOH-80. Reaction conditions: $P(H_2) = 0.1$ MPa, $T = 30$ °C, reaction time = 40 min, Pd = 1.6 μmol, phenylacetylene = 4.8 mmol, ethanol = 10 mL.

content *via* ICP-OES, we determined that the optimal loading amount of Pd for the Pd/AlOOH catalyst was 0.7 wt%, with significantly higher (1.5 wt%/2.5 wt%) or lower (0.3 wt%) loading amounts not favorably impacting catalytic activity (Fig. S5 and Table S2†).

This clarified the underlying reaction mechanism, highlighting the enhanced catalytic effect originating from ssFLP. The abundant ssFLP in AlOOH-80 facilitated the dissociation of hydrogen gas, enhancing the hydrogenation capability of Pd and resulting in Pd/AlOOH exhibiting remarkably high catalytic activity. Clearly, the Pd/AlOOH-80 catalyst derived its exceptional catalytic activity from ssFLP. Once ssFLP was damaged, the catalyst's ability to dissociate hydrogen diminished, and the original synergistic effect between Pd and AlOOH ceased to exist, significantly affecting the catalytic activity.

As widely acknowledged, Lewis acid or Lewis base sites were easily quenched by basic or acidic substances, respectively.[37,46] Therefore, we introduced benzoic acid or pyridine into the catalytic system to quench the Lewis base or Lewis acid sites, respectively, thereby disrupting the ssFLP. As shown in Fig. 6, the addition of benzoic acid to quench the Lewis basic sites led to a dramatic decrease in the catalytic activity of Pd/AlOOH, from 100% to 27.8%. Similarly, the addition of pyridine, quenching the Lewis acid sites, resulted in a significant reduction in the catalyst's activity, from 100% to 31.7%. However, the commercial Pd/Al_2O_3 catalyst was unaffected by the addition of either pyridine or benzoic acid.

All of these indicate that the ssFLP in Pd/AlOOH was the key to its ultra-high catalytic activity. Surprisingly, the larger-sized Pd nanoparticles (approximately 20 nm, Fig. 1c) in Pd/AlOOH demonstrated superior catalytic activity compared to the smaller-sized Pd nanoparticles in commercial Pd/Al_2O_3 (approximately 5.6 nm, Fig. S6†) and Pd/C (approximately 5.0 nm, Fig. S6†). This means that, with substantial assistance from ssFLPs, the synergistic effect between Pd and AlOOH, originating from ssFLPs, played a dominant role, rather than the size effect of nanoparticles.[47] Remarkably, Pd/AlOOH-80 exhibited exceptionally high catalytic activity, surpassing most reported catalysts (Table S3†). Furthermore, it demonstrated good reusability, showing no significant decline in catalytic performance over five experimental cycles, indicating its high potential for industrial applications (Fig. 7).

4. Conclusion

In summary, we successfully prepared layered AlOOH-80 using a simple method, facilitating the generation of OH defects for constructing ssFLP, which can be used for hydrogen dissociation. The hydrogen dissociation ability of ssFLP contributed to promoting the synergistic effect between Pd and AlOOH, significantly enhancing the catalytic performance of Pd/AlOOH-80, enabling it to exhibit exceptionally high catalytic activity. The analysis of AlOOH revealed that the performance of the catalyst was directly proportional to the number of OH defects in AlOOH and inversely proportional to the amount of adsorbed water. AlOOH-80, distinguished by its abundance of defects and minimal adsorbed water, presented an ideal condition for the formation of abundant ssFLPs. With the facilitation of ssFLP, the synergistic effect between Pd and AlOOH-80 was greatly enhanced. Consequently, Pd/AlOOH-80, the catalyst formed by loading Pd onto AlOOH-80, demonstrated markedly superior activity compared to Pd-based catalysts utilizing other oxide supports, even outperforming the commercial Pd/Al_2O_3 and Pd/C. Remarkably, larger-size Pd nanoparticles in Pd/AlOOH exhibited superior catalytic activity compared to the smallersize ones in commercial catalysts. This suggests that the dominant influence on catalytic performance was the synergistic effect between Pd and AlOOH, facilitated by ssFLPs, rather than the size effect of nanoparticles. Certainly, the role of ssFLP was crucial in the catalytic process. After ssFLP was quenched by pyridine/benzoic acid, the synergistic effect that enhanced the catalytic activity of the catalyst was disrupted, leading to an inevitable sharp decrease in the catalytic performance of Pd/AlOOH. Moreover, Pd/AlOOH-80 also showed good reusability, indicating its high potential for industrial applications.

Conflicts of interest

The authors declare no conflict of interest.

Acknowledgements

This work was supported by the National Natural Science Foundation of China (Grant 21904055) and the Natural Science Foundation of Fujian province (Grant 2023J011815, 2020J05164 and 2020J01807).

References

1 L. Lückemeier, M. Pierau and F. Glorius, *Chem. Soc. Rev.*, 2023, **52**, 4996–5012.
2 J. L. Wen, F. Y. Wang and X. M. Zhang, *Chem. Soc. Rev.*, 2021, **50**, 3211–3237.
3 M. A. Stevens and A. L. Colebatch, *Chem. Soc. Rev.*, 2022, **51**, 1881–1898.
4 C. Rivera-Cárcamo, I. Gerber, I. Del Rosal, B. Guicheret, R. C. Contreras, L. Vanoye, A. Favre-Réguillon, B. Machado, J. Audevard and C. De Bellefon, *Catal. Sci. Technol.*, 2021, **11**, 984–999.
5 R. F. Shen, Y. Y. Liu, H. Wen, T. Liu, Z. K. Peng, X. L. Wu, X. H. Ge, S. Mehdi, H. Q. Cao, E. R. Liang, J. C. Jiang and B. J. Li, *Appl. Catal., B*, 2022, **306**, 121100.
6 J. Sun, W. Xu, C. Lv, L. Zhang, M. Shakouri, Y. Peng, Q. Wang, X. Yang, D. Yuan and M. Huang, *Appl. Catal., B*, 2021, **286**, 119882.
7 C. Wallach, F. S. Geitner and T. F. Fässler, *Chem. Sci.*, 2021, **12**, 6969–6976.
8 D. Mahaut, B. Champagne and G. Berionni, *ChemCatChem*, 2022, **14**, e202200294.
9 M. Abdelgaid and G. Mpourmpakis, *ACS Catal.*, 2022, **12**, 4268–4289.
10 D. W. Stephan and G. Erker, *Angew. Chem., Int. Ed.*, 2010, **49**, 46–76.
11 D. W. Stephan, *Science*, 2016, **354**, aaf7229.
12 M. Miceli, P. Frontera, A. Macario and A. Malara, *Catalysts*, 2021, **11**, 591.
13 W. Nabgan, A. A. Jalil, B. Nabgan, A. H. Jadhav, M. Ikram, A. Ul-Hamid, M. W. Ali and N. S. Hassan, *RSC Adv.*, 2022, **12**, 1604–1627.
14 I. M. Atadashi, M. K. Aroua, A. R. A. Aziz and N. M. N. Sulaiman, *J. Ind. Eng. Chem.*, 2013, **19**, 14–26.
15 U. C. Rajesh, Divya and D. S. Rawat, *RSC Adv.*, 2014, **4**, 41323–41330.
16 Z. Hussain, Y.-A. Luo, Y. Wu, Z.-W. Qu, S. Grimme and D. W. Stephan, *Chem. Commun.*, 2023, **59**, 6191–6194.
17 Y. H. Wang, Z. H. Li and H. D. Wang, *RSC Adv.*, 2018, **8**, 26271–26276.
18 H. Zhang, X. Y. Zhan, Y. Dong, J. Yang, S. He, Z. C. Shi, X. M. Zhang and J. Y. Wang, *RSC Adv.*, 2020, **10**, 16942–16948.
19 D. R. Aireddy and K. Ding, *ACS Catal.*, 2022, **12**, 4707–4723.
20 S. L. Liu, M. H. Dong, Y. X. Wu, S. Luan, Y. Xin, J. Du, S. P. Li, H. Z. Liu and B. X. Han, *Nat. Commun.*, 2022, **13**, 2320.
21 R. R. Wei, Z. H. Gao and W. Huang, *Mol. Catal.*, 2023, **548**, 113457.
22 I. G. Nielsen, M. Kløve, M. Roelsgaard, A.-C. Dippel and B. B. Iversen, *Nanoscale*, 2023, **15**, 5284–5292.
23 H. Chai, J. Xu, Z. Zhang, J.-a. Lai, J. Wang, Z. Peng, K. Liu, C. Rao, X. Haijiao and Q. Liu, *Appl. Surf. Sci.*, 2024, 159709.
24 Z. Wang, Y. Huang, M. Chen, X. Shi, Y. Zhang, J. Cao, W. Ho and S. C. Lee, *ACS Appl. Mater. Interfaces*, 2019, **11**, 10651–10662.
25 J. Liao, W. Cui, J. Li, J. Sheng, H. Wang, P. Chen, G. Jiang, Z. Wang and F. Dong, *Chem. Eng. J.*, 2020, **379**, 122282.
26 Z. Tian, L. Wang, T. Shen, P. Yin, W. Da, Z. Qian, X. Zhao, G. Wang, Y. Yang and M. Wei, *Chem. Eng. J.*, 2023, **472**, 144876.
27 X. Shen, K. Kang, Z. Yu, W. H. Jeong, H. Choi, S. H. Park, S. D. Stranks, H. J. Snaith, R. H. Friend and B. R. Lee, *Joule*, 2023, **7**, 272–308.
28 M. I. Zaki, M. A. Hasan, F. A. Al-Sagheer and L. Pasupulety, *Colloids Surf., A*, 2001, **190**, 261–274.
29 B. Liu, H. J. Sun, T. J. Peng and J. Ma, *Appl. Surf. Sci.*, 2022, **579**, 152220.
30 X. G. Yin, Q. D. Zhu, Y. J. Tan, S. Y. Long, Y. Huang, Y. Li and X. L. Pei, *Appl. Surf. Sci.*, 2024, **648**, 159047.
31 H. Cao, R. Wang, K. Dou, J. Qiu, C. Peng, N. Tsidaeva and W. Wang, *Environ. Res.*, 2023, **216**, 114730.
32 C. Z. Wang, L. P. Han, Q. F. Zhang, Y. K. Li, G. F. Zhao, Y. Liu and Y. Lu, *Green Chem.*, 2015, **17**, 3762–3765.
33 J. G. Ren, H. B. Weng, B. Li, F. Chen, J. B. Liu and Z. M. Song, *Front. Earth Sci.*, 2022, **10**, 841353.
34 C. F. Toncón-Leal, J. Villarroel-Rocha, M. T. P. Silva, T. P. Braga and K. Sapag, *Adsorption*, 2021, **27**, 1109–1122.
35 F. Salimi, M. Abdollahifar and A. R. Karami, *Ceram.-Silik.*, 2016, **60**, 273–277.
36 J. Hu, Y. Li, Y. Zhen, M. Chen and H. Wan, *Chin. J. Catal.*, 2021, **42**, 367–375.
37 S. Liu, M. Dong, Y. Wu, S. Luan, Y. Xin, J. Du, S. Li, H. Liu and B. Han, *Nat. Commun.*, 2022, **13**, 2320.
38 Z. Xu, J. Yu and M. Jaroniec, *Appl. Catal., B*, 2015, **163**, 306–312.
39 J. Li, W. Suo, Y. Huang, M. Chen, H. Ma, C. Liu, H. Zhang, K. Liang and Z. Dong, *J. Colloid Interface Sci.*, 2023, **652**, 1053–1062.
40 X. Zhang, Q. Gu, Y. Ma, Q. Guan, R. Jin, H. Wang, B. Yang and J. Lu, *J. Catal.*, 2021, **400**, 173–183.

41 X. Liu, J. N. McPherson, C. E. Andersen, M. S. B. Jørgensen, R. W. Larsen, N. J. Yutronkie, F. Wilhelm, A. Rogalev, M. Giménez-Marqués, G. Mínguez Espallargas, C. R. Göb and K. S. Pedersen, *Nat. Commun.*, 2024, **15**, 1177.
42 Z. Yan, Z. Xu, J. Yu and M. Jaroniec, *J. Colloid Interface Sci.*, 2017, **501**, 164–174.
43 S. Zhang, Z.-Q. Huang, Y. Ma, W. Gao, J. Li, F. Cao, L. Li, C.-R. Chang and Y. Qu, *Nat. Commun.*, 2017, **8**, 15266.
44 A. Baccarella, R. Garrard, M. Beauvais, U. Bednarksi, S. Fischer, A. M. Abeykoon, K. Chapman, B. Phillips, J. Parise and J. Simonson, *J. Solid State Chem.*, 2021, **301**, 122340.
45 B. Dargatz, J. Gonzalez-Julian, M. Bram, P. Jakes, A. Besmehn, L. Schade, R. Röder, C. Ronning and O. Guillon, *J. Eur. Ceram. Soc.*, 2016, **36**, 1207–1220.
46 K. K. Ghuman, L. B. Hoch, P. Szymanski, J. Y. Loh, N. P. Kherani, M. A. El-Sayed, G. A. Ozin and C. V. Singh, *J. Am. Chem. Soc.*, 2016, **138**, 1206–1214.
47 K. Murata, Y. Mahara, J. Ohyama, Y. Yamamoto, S. Arai and A. Satsuma, *Angew. Chem.*, 2017, **129**, 16209–16213.